Silver mesostructures and core/shell structures (Au/AgNRs) for anti-bacterial effect

Do Thi Hue

Thai Nguyen University of Education, No. 20, Luong Ngoc Quyen street, Quang Trung ward, Thai Nguyen city, Thai Nguyen province, Viet Nam

Email: huedt@tnue.edu.vn

Abstract. A systematic and detailed study of the antibacterial efficacy of silver nanoparticles (AgNPs) with different structures synthesized by chemical methods is presented here. Silver mesostructures are synthesized in the presence of the weak reducing agent L-ascorbic acid (L-AA). Meatball-like unbranched mesostructures and coral-like branched nanostructures were obtained by adjusting precursor concentration $AgNO_3$. The core/shell structures (Au/AgNRs) with controlled shells were prepared according to the seed growth method using gold nanorods (AuRs) as the hard template. The influence of silver nanoparticle's structure on antibacterial activity was investigated with different concentrations of the silver nanoparticles on two types of bacteria (*P.aeruginosa* and *S. aureus*) resistance while a positive control was *Ampicillin* 50 mg/mL. The results show that all samples had antibacterial properties comparable to or superior to those of *Ampicillin*. At the concentration of particles of 50 μg/mL, the antibacterial performance is the highest. The more branched structure, and the higher the antibacterial ability.

Keywords: Antibacterial activity, silver nanoparticles, AgNPs, Au/AgNRs, mesostructures.

Classification numbers: 2.4.2, 2.4.4.

1. INTRODUCTION

Silver nanostructures have become widely used materials in the field of nanoscience and technology because of their attractive properties. With plasmon resonance frequencies located in the visible light region and their strong antibacterial and anti-inflammatory properties, the silver nanoparticles offer a wide range of applications in the fields of physics, biology, and different pharmacy products [1 - 3]. Currently, on the market, many products use silver nanoparticles as the main ingredient to create the brand of the product, such as anti-inflammatory drug products, antibacterial solutions, even electronic devices, and water treatment as well. Besides, the silver nanostructures have gained much attention due to their various applications in the areas of sensor engineering, catalysis, and surface-enhanced Raman scattering (SERS) [4 - 7]. The silver nanostructures' optical properties and consequent applications depend strongly on their shape, structure, and size. Therefore, many publications have related to synthesizing silver nanoparticles with different shapes and sizes, such as spheres, triangles, plates, wires, cubes and so on [8 - 12]. Which, there are many publications using L-AA as a reducing agent for Ag^+ ions [13 - 15].

The silver nanostructures have antibacterial activity in two ways: inhibiting bacterial growth by blocking nutrient channels in cell membranes and killing bacteria by damaging their cell membranes [3, 16 - 22]. Silver ion (Ag^+) has a very strong attraction to negatively charged functional groups in the molecular biological structure of bacterial cells, such as -SH, -COOH groups, etc. Thanks to that, it can break bonds and change the structure of bacterial cells, preventing metabolism with the growth medium. Silver's bactericidal properties occur almost immediately with single-celled organisms such as bacteria and viruses. The silver nanoparticles with more surface area, more chemical reactivity, and thereby increased antibacterial ability many times. The antibacterial properties of silver nanoparticles are strong or weak depending mainly on their structure, shape, and size. Therefore, in this work, we systematically study the antibacterial properties of silver nanoparticles of different shapes based on the materials we have synthesized.

To investigate the influence of the shape and structure of silver nanoparticles on antibacterial ability, we compared the antibacterial performance of silver nanoparticles with different shapes such as a sphere, meso silver structures (branched and unbranched), and core-structured silver nanorods Au/AgNRs shell with the same concentrations.

2. MATERIALS AND METHODS

2.1. Chemicals

Silver nitrate ($AgNO_3$, > 99 %) and L-ascorbic acid (L-AA, 99 %) were purchased from Sigma Aldrich; Gold (III) chloride trihydrate ($HAuCl_4 \cdot 3H_2O$, ≥ 99.9 %), cetyltrimethylammonium bromide (CTAB, ≥ 99 %) and cetyltrimethylammonium chloride (CTAC, 25 %) were purchased from Merck, Germany. Chemicals were used without any further purification. The deionized water (DI) with a resistance of 18.2 MΩ was used in all processes.

2.2. Synthesis of Silver nanostructures

Silver mesostructures were synthesized by the chemical reduction method in the presence of the weak reducing agent L-ascorbic acid (L-AA) [11,23]. To synthesize silver mesostructures with different branching, volumes of $AgNO_3$ were used such that the final concentrations of the Ag^+ ions were determined to be 1.5 mM, and 0.1 mM. 800 µL of 0.4 M L-AA was then added to the $AgNO_3$ solution while gently stirring at a rate of 300 rpm at 30°C. The color of the solution changed from colorless to light grey after 10 min and did not change then after. The reaction was maintained for about 20 min to ultimately reduce Ag^+ ions to Ag^0 atoms. The obtained silver mesostructures were cleaned by centrifugation 3 times at 6000 rpm for about 30 min each time.

The core/shell structures (AuR/Ag) were prepared according to the seed growth method with the use of gold nanorods as the hard template [24 - 26]. 10 mL of the gold nanorod solution was centrifuged 3 times to remove all CTAB, then redispersed in 0.08 M CTAC solution to keep the particle concentration unchanged. Add a volume of 0.01 M $AgNO_3$ solution to the gold nanorod solution. Then, 0.1 M L-AA solution was put into the reaction vessel with a volume equal to half the volume of $AgNO_3$ solution. To synthesize core/shell structures with variable thickness of Ag shell, the volumes of $AgNO_3$ solution were 2 mL (S1) and 0.05 mL (S2), respectively. The solution mixture was incubated in a 65°C isothermal oven for 4.5 h.

2.3. Antibacterial tests

The antimicrobial activity of nanoparticles was determined using the disc diffusion method. All bacteria were cultured in a nutrient agar medium at 37 ℃ with continuous shaking at 200

rpm for 24 h. The microorganism suspensions were diluted with sterile distilled water and adjusted to approximately 108 colony-forming units per milliliter (CFU/mL) using standard curves at OD 600. 0.1 mL of the diluted microorganism suspension was streaked onto the plate with mL nutrient agar medium. The serial dilutions were conducted with different concentrations of 12.5 µg/mL, 25 µg/mL, and 50 µg/mL of gold nanoparticles. After adding 50 µL solutions to each well in agar (diameter 6 mm), the dishes were kept for 1 h at 4°C. The bacteria P.aeruginosa (P.A) and S. aureus (S.A) were incubated at 37 ℃ for 24 h. After the incubation period, the zone growth of the plate incubation was observed after 14 h. The used negative control was water without test material, while the positive control was Ampicillin 50 µg/mL. The experiments were performed in triplicate.

2.4. Characterization

The morphology of the silver nanostructures was characterized using scanning electron microscopy (SEM) (JEOL JSM-7000F) at an accelerating voltage of 20 kV and transmission electron microscopy (TEM) (JEOL JEM-2100) at an accelerating voltage of 200 kV. The absorption spectrum using a Jasco V-770 UV–Vis spectrophotometer in the range of 250 nm – 1000 nm was used to produce the optical properties of silver nanostructures. The structure, composition, and physical properties of the silver mesostructures were studied by the XRD. The XRD spectra using an X-ray diffractometer (Bruker D8 Advance, Germany) allow for determining the morphological and structural features of the particles. This device worked at 30 kV with Cu-Kα radiation (wavelength of λ = 0.154 056 nm) with parallel-beam geometry between 30° to 80° range. For XRD analysis, the solutions were reduced on a glass substrate to a spot with a diameter of about 0.5 cm to obtain a sufficiently thick layer.

3. RESULTS AND DISCUSSION

3.1. Silver mesostructures

Silver nanoparticles up to several hundred nanometers in size with different branched structures were synthesized using the environmentally friendly, green reducing agent L-AA. By varying the $AgNO_3$ precursor concentration, coral-like and meatball-like silver mesostructures were formed (Figure 1). The silver mesostructures are relatively uniform in shape and size. When the concentration of precursors in the solution is large, the silver mesostructures have an unbranched structure that is meatball-like with a relatively rough surface, the average size of the particles is about 250 nm. In contrast, when the concentration of $AgNO_3$ in the solution decreased to 0.1 mM, a branched structure was formed, and the branches grew indifferent, but in relatively uniform directions, forming a coral-like structure. The degree of branching and growth of the branches became more and more intense as the precursor concentration decreased as in our previous report [21]. The mechanism of the development of these structures is illustrated by the Lamer diagram and has been clearly explained in our previous report [21]. This can be briefly rephrased as follows: the formation of different silver mesostructures is due to kinetic mechanisms during the formation and growth of particles in solution according to the phases of the Lamer mechanism. With different structures, the silver mesostructures have their characteristic optical properties, which are shown by the appearance of additional plasmon resonance peaks in the ultraviolet side for coral-branched structures (Figure 1c). The optical properties of the silver mesostructures depend on their morphology. Depending on the distribution of electrons on the particle surface, their interaction with the excitation light will induce different plasmon resonance oscillations forming characteristic vibrational modes. The higher-order oscillation modes contributed by electrons distributed on the branches of the silver

meso-structure correspond to the higher energies. For the meatball-like structure, in addition to dipole resonance, there is an additional quadrupole resonance and an octopole resonance. For the coral-like structure, the geometric symmetry is lower, so under the effect of the electromagnetic field, more vibration modes will appear, forming plasmon resonance peaks corresponding to the geometrical structures of the particle [27]. The positions of dipole, quadrupole and octopole resonance shift to wavelengths of 650 nm, 445 nm and 350 nm, respectively.
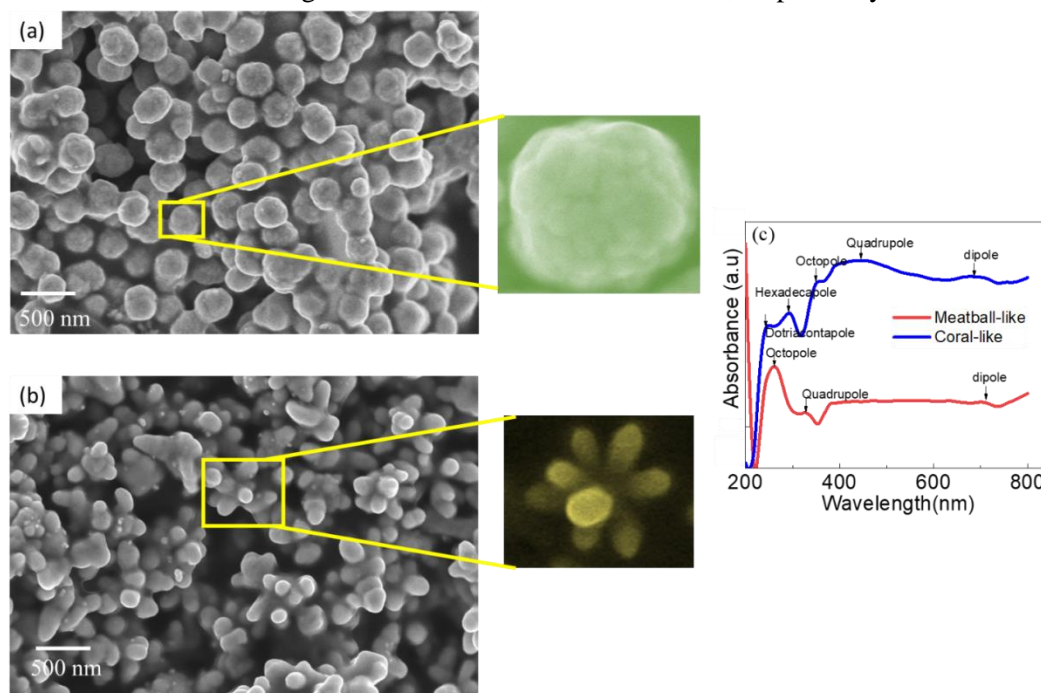
Figure 1. SEM images of silver mesostructures with $AgNO_3$ concentrations 1.5 mM (a), 0.1 mM (b); and their UV-Vis absorption spectra (c). The images inserted are enlarged images of silver mesostructures.

3.2. Core/shell structures (Au/AgNRs)

Another structure of silver nanoparticles that have also been synthesized to study its antibacterial properties is the core/shell structure (Au/AgNR). This is a multilayer structure with a core of gold nanorods and a silver shell. The thickness of the silver shell was adjusted by varying the $AgNO_3$ concentration during shell formation. The results showed that Au/AgNRs core/shell structures were formed, the silver shell uniformly surrounded the gold nanorod, and the thicker the shell the more $AgNO_3$ solution concentration (Figure 2 a,b). The shell sample S1 is about 7 nm thick while the shell sample S2 is only about 3 nm thick. The samples S1, S2 have aspect ratios of 3 and 7 correspondingly. The significant change in optical properties when the shell is formed can be seen through the plasmon absorption spectra of the gold nanorods and the Au/AgNRs core/shell structures (Figure 2d). The optical properties of the Au/AgNRs core/shell structures are due to the contribution of the collective oscillations of the electrons on the Ag shell and the interaction of the electrons between the Ag shell and AuR core. The absorption spectra of the gold nanorods with two resonance peaks at 526 nm and 573 nm characterize the collective oscillation of the transverse and long electrons of the rod. The short-wavelength oscillation modes are attributed to the contribution of electrons oscillating in the horizontal direction of the rod. In the Au/AgNRs structures, this mode of oscillation is mainly due to the electrons in the Ag shell. It is equivalent to the dipole oscillation of a nanosphere. The thinner

the shell (the smaller the silver nanosphere size), the more the plasmon resonance peak shifts towards the short wave. Therefore, the horizontal plasmon resonance peak of S2 shifts towards the short wave relative to S1. When the shell is thick enough, the interaction of the electrons on the Ag shell and the electrons on the AuR core becomes important, forming high-energy high-order vibrational modes. Therefore, on the S1 spectrum, there are resonance peaks in the near-ultraviolet region. At the same time, the resonance peaks that characterize the oscillations of the rods also shift towards the short wave. This is because when the core/shell structure is formed, the growth of the silver shell at the ends of the rods is always slower than at the sides of the rods. So as the shell becomes thicker, the ratio of the sides of the rod decreases.

The formation of the Ag shell on the AuR core is a complex process that includes three stages: The first stage is the formation of the Ag^+@micelle complex by diffusing the CTAC surfactant and Ag^+ ions which are produced from $AgNO_3$. The second stage is the formation of a double shell on the AuR surface under the direction of the Ag^+@micelle complex. The final stage is the reduction of Ag^+ on different faces of AuR creating anisotropic development of the shell [28]. CTAC surface molecules with the Cl^- group are more associated with the {111} faces (at the ends of the rod) than with the {110} or {100} sides [28]. Therefore, Ag^+ ions are reduced more at the side faces than at the ends of the rod. This reduces the aspect ratio of the bar structure.
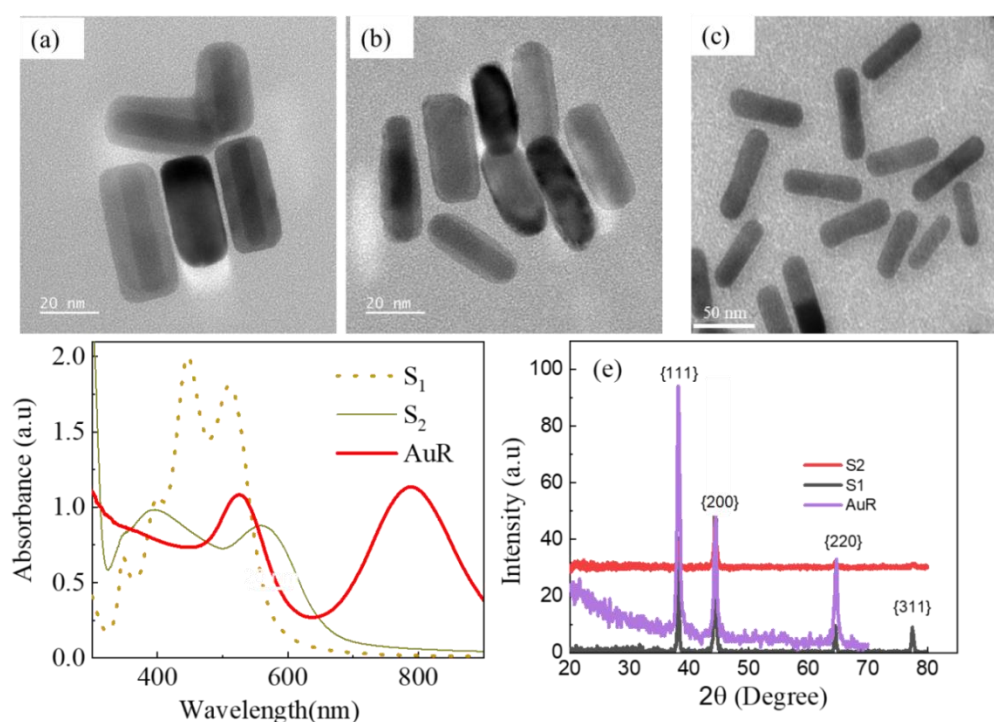
Figure 2. TEM images of Au/AgNRs (a – S1, b – S2) core/shell structures, of gold nanorods (c), plasmon absorption spectra of gold nanorods and Au/AgNRs (d), X-ray diffraction patterns of Au/AgNRs (S1 and S2) and AuR (e).

The higher the $AgNO_3$ concentration, the more Ag^+ is reduced, so the Ag shell is thicker. According to Gans's theory, this results in resonance peaks shifting towards the short wave [29]. The X-ray diffraction patterns of the AuR and Au/AgNRs structures are shown in Figure 2e. The

diffraction peaks at 2θ positions are 38.3°, 44.3°, 64.6°, and 77.6° for the {111}, {200}, {220} and {311} crystal planes, respectively. From the XRD, only one set of reflection planes is obtained for both the AuR cores and the Au/AgNRs. Au and Ag have fcc crystal structures with relatively similar lattice constants (JCPDF standard: 04-0783 and 04-0784). This plays an important role in the formation of a homogeneous Ag shell. Furthermore, in addition to the condensed crystal planes of Au and Ag, there are no additional diffraction peaks. This shows that the core/shell structures have good crystalline quality (Figure 2e).

3.3. Antibacterial application

3.3.1. Effect of silver nanostructure on antibacterial properties

Regarding the influence of silver nanostructures on antibacterial properties, silver nanoparticles with different structures were used: Au/AgNRs core/shell nanostructure, meatball-like mesostructures, and coral-like mesostructures (Figure 3). The results showed that all samples had antibacterial activity against the tested bacteria, and the inhibitory activity was highest at the concentration of 50 μg/mL (Figure 3). Different structures have different antibacterial activity but are all better or equivalent to antibacterial activity when using Amp antibiotic. Comparing samples with the same concentration of 50 μg/mL, and 25 μg/mL, it can be seen that the antibacterial ability increases in the order: thick shell- Au/AgNRs, thin shell-Au/AgNRs, meatball-like, and coral-like structure. This is explained by the better mechanism of releasing Ag ions of the mesostructures than rod structures, in which the coral structure with many hotspots has the best ability to release Ag ions. These results are also shown in

Figure *4* with the difference in the width of the sterile rings. The maximum diameter of the aseptic ring for S. aureus was 12 mm when using a meatball-like structure and 14 mm for *P.aeruginosa* (P.A) when using a coral-like structure.
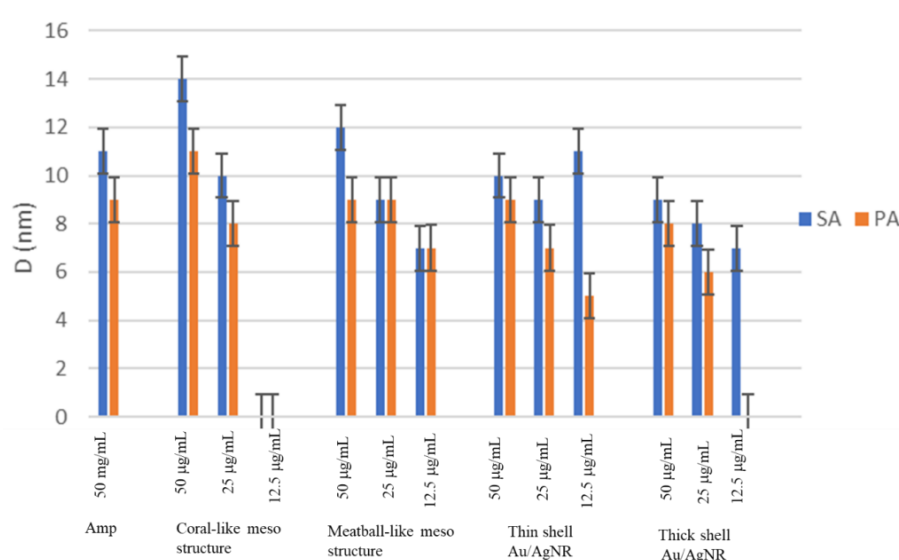
Figure 3. The dependence of antibacterial zone diameter on the structure of silver nanoparticles.

The results show that thin-shell Au/AgNRs with a concentration of 12.5 μg/mL exhibit better P.A antibacterial activity at high concentrations. In our opinion, the Au/AgNRs structures

with thin shells kill bacteria mainly due to the penetration of silver nanoparticles into the cell. This depends on the exposure of Au/AgNRs to the cell. When the concentration of thin-shell Au/AgNRs decreased to some extent (12.5 µg/mL - according to our survey), the exposure of Au/AgNRs structures to the cell membrane increased more efficiently antibacterial capacity. However, the antibacterial mechanism of Au/AgNRs structures is still unclear and requires further studies.
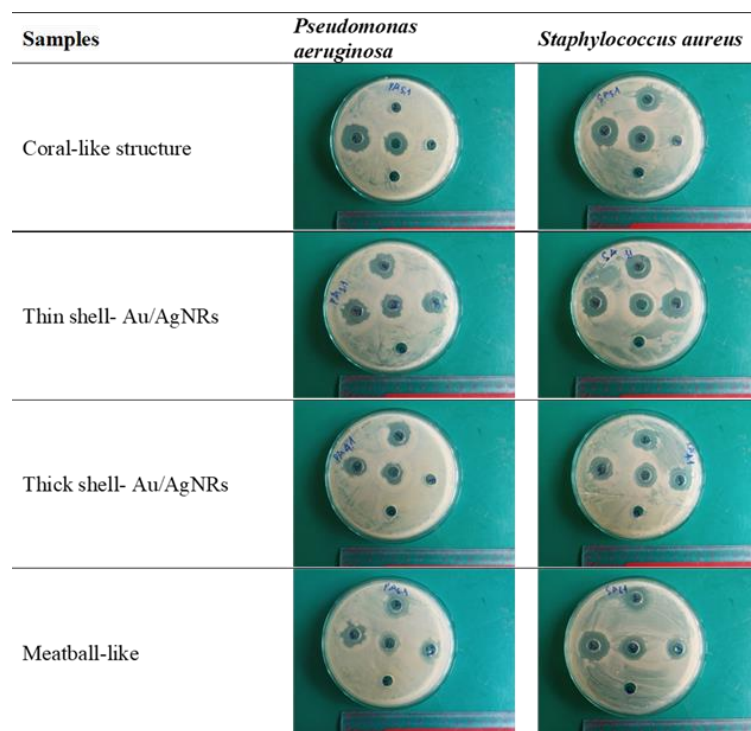
Figure 4. P.aeruginosa and *S. aureus* resistant rounds using different silver nanostructures.

3.3.2. Antibacterial mechanism of silver nanoparticles

The antibacterial mechanism of silver nanoparticles is due to two main factors that interfere with cells. The first is the release of Ag^+ ions from silver nanoparticles, which creates electrostatic and affinity binding forces with the cell's sulfur proteins, causing Ag^+ ions to penetrate the cell membrane and cytoplasm, breaking it down the cell membrane, and bacterial envelope [16, 17, 21, 22]. Penetration of Ag^+ ions can also cause protein inhibition by denaturing ribosomes [17]. The interaction of silver ions with sulfur and phosphorus in DNA can cause problems in DNA replication, and cell multiplication or even lead to the destruction of microorganisms [30]. In addition, Ag^+ ions can inactivate respiratory enzymes on the cytoplasmic membrane. Second, the penetration of silver nanoparticles into the cell membrane can cause accumulation in the pores in the cell membrane that denature the cell membrane or perforate the cell membrane [16, 17, 30]. In addition, silver nanoparticles have the ability to interrupt bacterial signal transduction by phosphorylation of protein substrates, and dephosphorylate tyrosine residues on peptide substrates. Interrupting signal transduction terminates cell replication. All these mechanisms are shown in Figure 5.

The release of Ag^+ ions as well as the ability of silver nanoparticles to diffuse and penetrate the cell membrane to kill bacteria depends on the concentration, surface activity of the particles,

and the shape and size of the silver nanoparticles. The spherical or semicircular particles are better able to release Ag^+ ions. At the same time, particles of the same volume with a large surface area have a better antibacterial ability. This explains why the smaller the spherical silver nanoparticles, the better the ability to kill bacteria. The antibacterial mechanism of silver mesoporous particles can be explained by the fact that the Ag^+ ion release of the branched structures with many "hot spots" is better than the Ag^+ ion release of the unbranched structures. The Au/AgNRs structures are smaller in size but have fewer "hot spots" than the Ag mesostructures. Therefore, the combination of the Ag^+ release mechanism and the penetration of silver nanoparticles into the cell forms the antibacterial mechanism of Au/AgNRs.
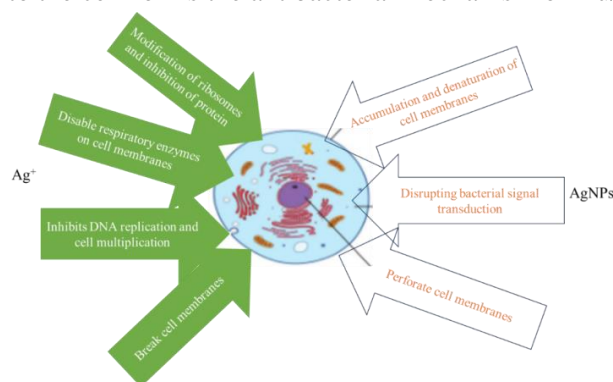
Figure 5. Antibacterial mechanisms of silver nanoparticles.

4. CONCLUSIONS

Different structures of silver nanoparticles have been synthesized in a controlled manner, from mesostructure to core/shell structures. The silver mesostructures with a size over 200 nm in the form of meatball-like mesostructures were obtained when the concentration of $AgNO_3$ was 1.5 mM and the coral-like mesostructures were obtained when the concentration of $AgNO_3$ was 0.1 mM. The Au/AgNRs core/shell structures are relatively uniform in shape and size with shell thicknesses from 3 nm to 7 nm as the $AgNO_3$ volume increases from 0.05 mL to 2 mL. The results showed that all samples were capable of antibacterial capacity by surveying the antibacterial properties of the fabricated materials on the bacteria *P.aeruginosa* and *S. aureus* resistance and comparing with the antibacterial ability of *Amp*-specific antibiotics equivalent and even higher than *Amp*. With a particle concentration of 50 µg/mL, the antibacterial effect was highest and this efficiency depended on the structure of the particles. The coral-like mesostructures had the best antibacterial effect. This is explained by the ability to release Ag^+ ions from the hotspots of the branched structures in the silver mesostructures.

Declaration of competing interest. The author declares that she has no known competing financial interests or personal relationships that could have appeared to influence the work reported in this paper.

REFERENCES

1. Nakamura S., Sato M., Sato Y., Ando N., Takayama T., Fujita M., Ishihara M. - Synthesis and application of silver nanoparticles (Ag nps) for the prevention of infection in healthcare workers, International Journal of Molecular Sciences **20** (15) (2019). doi:10.3390/ijms20153620

2. Bapat R. A., Chaubal T. V., Joshi C. P., Bapat P. R., Choudhury H., Pandey M., Gorain B, Kesharwani P. - An overview of application of silver nanoparticles for biomaterials in dentistry, Materials Science and Engineering C **91** (2018) 881-898. doi:10.1016/j.msec.2018.05.069

3. Yin I.X., Zhang J., Zhao I.S., Mei M.L., Li Q., Chu C.H. - The antibacterial mechanism of silver nanoparticles and its application in dentistry, International Journal of Nanomedicine **15** (2020) 2555-2562. doi:10.2147/IJN.S246764

4. Novikov S. M., Popok V. N., Evlyukhin A. B., Hanif M., Morgen P., Fiutowski J., Beermann H. G., Rubahn J., and Bozhevolnyi S. I. - Highly stable silver nanoparticles for SERS applications, Journal of Physics: Conference Series, Institute of Physics Publishing **1092** (2018) 012098. doi:10.1088/1742-6596/1092/1/012098

5. Pilot R., Massari M. - Silver nanoparticle aggregates: Wavelength dependence of their SERS properties in the first transparency window of biological tissues, Chemical Physics Impact. **2** (2021) 100014. doi:10.1016/j.chphi.2021.100014

6. Guo H., Zhang Z., Xing B., Mukherjee A., Musante C., White J.C., He L. -Analysis of silver nanoparticles in antimicrobial products using surface-enhanced raman spectroscopy (SERS), Environ Sci. Technol. **49** (7) (2015) 4317-4324. doi:10.1021/acs.est.5b00370

7. Babu S., Srijith S., Resmi S. - Silver nanoparticles as surface enhanced Raman scattering (SERS) substrates, In: AIP Conference Proceedings, American Institute of Physics Inc. **2379,** 2021, pp. 247. doi:10.1063/5.0058247

8. Khodashenas B., Ghorbani H.R. - Synthesis of silver nanoparticles with different shapes, Arabian Journal of Chemistry **12** (8) (2019) 1823-1838. doi:10.1016/j.arabjc.2014.12.014

9. Guilger-Casagrande M., Lima R. de. - Synthesis of Silver Nanoparticles Mediated by Fungi: A Review, Front Bioeng Biotechnol. **7** (2019) 287. doi:10.3389/fbioe.2019.00287

10. Ferrag C., Li S., Jeon K., Andoy N. M., Sullan R. M. A., Mikhaylichenko S., Kerman K. - Polyacrylamide hydrogels doped with different shapes of silver nanoparticles: Antibacterial and mechanical properties, Colloids Surf B Biointerfaces **197** (2021) 397. doi:10.1016/j.colsurfb.2020.111397

11. Hue D. T., Thao N. T. P., Khoi T. K., Ha C. V. - Multi-shaped silver meso-particles with tunable morphology for surface enhanced Raman scattering, Opt. Commun. **497** (2021) 127200. doi:10.1016/j.optcom.2021.127200

12. Soleimani F. F., Saleh T., Shojaosadati S. A., Poursalehi R. - Green Synthesis of Different Shapes of Silver Nanostructures and Evaluation of Their Antibacterial and Cytotoxic Activity, Bionanoscience **8** (1) (2018) 72-80. doi:10.1007/s12668-017-0423-1

13. Tyagi P. K., Tyagi S., Gola D., Arya A., Ayatollahi S.A., Alshehri M. M., Sharifi-Rad J. - Ascorbic Acid and Polyphenols Mediated Green Synthesis of Silver Nanoparticles from Tagetes erecta L. Aqueous Leaf Extract and Studied Their Antioxidant Properties, J. Nanomaterial **2021** (2021) 1-9. https://doi.org/10.1155/2021/6515419

14. Chekin F., Ghasemi S. - Silver nanoparticles prepared in presence of ascorbic acid and gelatin, and their electrocatalytic application, Bulletin of Materials Science **37** (2014) 1433-1437 (2014). https://doi.org/10.1007/s12034-014-0093-3

15. Rathore G., Gupta A., Singh L. - An eco-friendly approach for fabrication of silver nanoparticles by using ascorbic acid from various native sources, International Journal of

Pharmaceutical Research **12** (2) (2020) 41-8. DOI:https://doi.org/10.31838/ijpr/2020.12.02.0002

16. Tang S., Zheng J. - Antibacterial Activity of Silver Nanoparticles: Structural Effects, Adv, Healthc Mater. **7** (13) (2018) 1503. doi:10.1002/adhm.201701503

17. Qing Y., Cheng L., Li R., Liu G., Zhang Y., Tang X., Wang J., Liu H., Qin Y. - Potential antibacterial mechanism of silver nanoparticles and the optimization of orthopedic implants by advanced modification technologies, Int, J. Nanomedicine **13** (2018) 3311-3327. doi:10.2147/IJN.S165125

18. Islam M. S., Naz A. N., Alam M. N., Das A. K., Yeum J. H. - Electrospun poly(vinyl alcohol)/silver nanoparticle/carbon nanotube multi-composite nanofiber mat: Fabrication, characterization and evaluation of thermal, mechanical and antibacterial properties, Colloids and Interface Science Communications **35** (2020) doi:10.1016/j.colcom.2020.100247

19. Urnukhsaikhan E., Bold B. E., Gunbileg A., Sukhbaatar N., Mishig-Ochir T. - Antibacterial activity and characteristics of silver nanoparticles biosynthesized from Carduus crispus, Sci Rep. **11** (1) (2021). doi:10.1038/s41598-021-00520-2

20. Dutta T., Ghosh N. N., Das M., Adhikary R., Mandal V., Chattopadhyay A. P. - Green synthesis of antibacterial and antifungal silver nanoparticles using Citrus limetta peel extract: Experimental and theoretical studies, J, Environ Chem, Eng. **8** (4) (2020) doi:10.1016/j.jece.2020.104019

21. Gomes H. I. O., Martins C. S. M., Prior J. A. V. - Silver nanoparticles as carriers of anticancer drugs for efficient target treatment of cancer cells, Nanomaterials **11** (4) (2021) doi:10.3390/nano11040964

22. Noorbazargan H., Amintehrani S., Dolatabadi A., Mashayekhi A., Khayam N., Moulavi P., Naghizadeh M., Mirzaie A., Rad F M., Kavousi M. - Anti-cancer & anti-metastasis properties of bioorganic-capped silver nanoparticles fabricated from Juniperus chinensis extract against lung cancer cells, AMB Express **11** (1) (2021). doi:10.1186/s13568-021-01216-6

23. Xu M., Zhang Y. - Hierarchical Ag mesostructures for single particle SERS substrate. Appl Surf Sci. **393** (2017) 197-203. doi:10.1016/j.apsusc.2016.10.011

24. Liu M., Guyot-Sionnest P. - Synthesis and optical characterization of Au/Ag core/shell nanorods, Journal of Physical Chemistry B **108** (19) (2004) 5882-5888. doi:10.1021/jp037644o

25. Jayabal S., Ramaraj R. - Synthesis of core/shell Au/Ag nanorods embedded in functionalized silicate sol-gel matrix and their applications in electrochemical sensors, Electrochim Acta. **88** (2013) 51-58. doi:10.1016/j.electacta.2012.10.065

26. Gorbunova M.V., Apyari V.V., Dmitrienko S.G, Garshev A.V. - Formation of core-shell Au@Ag nanorods induced by catecholamines: A comparative study and an analytical application, Anal Chim Acta **936** (2016) 185-194. doi:10.1016/j.aca.2016.07.038

27. Hue D. T., Thao N. T. P., Khoi T. K., Ha C. V. - Multi-shaped silver meso-particles with tunable morphology for surface enhanced Raman scattering, Opt. Commun. **497** (2021) 127200. https://doi.org/10.1016/j.optcom.2021.127200

28. Tebbe M., Kuttner C., Mayer M., Maennel M., Pazos-Perez N., König T.A.F., Fery A. - Silver-Overgrowth-Induced Changes in Intrinsic Optical Properties of Gold Nanorods:

From Noninvasive Monitoring of Growth Kinetics to Tailoring Internal Mirror Charges, Journal of Physical Chemistry C **119** (17) (2015) 9513-23. https://doi.org/10.1021/ acs.jpcc.5b03155

29. Ranjan M. - Predicting plasmonic coupling with Mie-Gans theory in silver nanoparticle arrays, Journal of Nanoparticle Research **15** (9) (2013). doi:10.1007/s11051-013-1908-7

30. Islam M. S., Naz A. N., Alam M. N., Das A. K., Yeum J. H. - Electrospun poly(vinyl alcohol)/silver nanoparticle/carbon nanotube multi-composite nanofiber mat: Fabrication, characterization and evaluation of thermal, mechanical and antibacterial properties, Colloids and Interface Science Communications **35** (2020). doi:10.1016/j.colcom. 2020.100247